Multiscale finite element and domain decomposition methods for high-contrast problems using local spectral basis functions

Yalchin Efendiev* Juan Galvis† Xiao-Hui Wu‡

Abstract

In this paper, we study multiscale finite element methods (MsFEMs) using basis functions that provide an optimal convergence in domain decomposition methods. We consider second order elliptic equations with highly variable coefficients. Both multiscale finite element and domain decomposition methods (considered here) use coarse spaces to achieve efficiency and robustness. In MsFEMs, the spatial variability of the media affects the convergence rate (see e.g., [14]). In domain decomposition methods, high variability of the coefficients within coarse regions affects the number of iterations required for the convergence. In this paper, we use coarse spaces designed for high-contrast problems that provide an optimal convergence in domain decomposition methods. These spaces are constructed locally. In particular, basis functions are constructed using solutions of a local spectral problem. In our previous work [18], we show that using these coarse spaces one can construct preconditioners such that the condition number of the preconditioned system is independent of the contrast. In this paper, these coarse spaces are used in MsFEMs to solve elliptic equations with high-contrast heterogeneous coefficients on a coarse grid. Our numerical results show that MsFEMs with coarse spaces constructed via local spectral problems are more accurate compared to multiscale methods that employ traditional multiscale spaces, e.g., with linear boundary conditions. However, we argue that these coarse spaces based on local eigenvalue problems are not sufficient to capture the fine-scale behavior of the solution very accurately. In particular, these coarse spaces identify high conducting regions accurately, but they may not capture the detailed behavior of the solution in other regions, such as between high-conductivity regions. The latter can be important for the

*Department of Mathematics, Texas A & M University, College Station, TX 77843 (efendiev@math.tamu.edu)

†Department of Mathematics, Texas A & M University, College Station, TX 77843 (jugal@math.tamu.edu)

‡ExxonMobil Upstream Research Company, P.O. Box 2189, Houston, TX 77252 (xiao-hui.wu@exxonmobil.com)

convergence of MsFEMs. In the paper, we also show that one can construct coarse spaces hierarchically by approximating the eigenvectors on a coarse grid. This approximation, though does not reduce the dimension of the coarse space, it provides CPU savings. The numerical results are presented for both MsFEMs and domain decomposition methods for the sake of completeness.

1 Introduction

Subsurface properties typically vary several orders of magnitude over multiple scales. A high contrast in the media properties brings an additional small scale into the problem expressed as the ratio between low and high conductivity values. For example, it is very common to have several orders of magnitude of variations in the permeability field in natural porous formations. It is common to use upscaled or multiscale models to solve flow and transport processes on the coarse grid [23, 1, 2, 4, 5, 6, 10, 11, 13, 25]. These approaches approximate the effects of the fine-scale features and attempt to capture their effects on a coarse grid via localized basis functions. The main idea of the MsFEM is to construct basis functions that are used to approximate the solution on a coarse grid. It is found the accuracy of MsFEMs is very sensitive to the boundary conditions imposed in computing basis functions (e.g., [14]).

Domain decomposition methods (considered in this paper), on the other hand, use the solutions of local problems in constructing preconditioners for the fine-scale system. Both MsFEMs and domain decomposition methods employ coarse spaces to achieve efficiency and robustness. The number of iterations required by domain decomposition preconditioners is typically affected by the contrast in the media properties that are within each coarse grid block. In [18], we introduce a coarse space based on local spectral problems (see also [9, 28]). These spaces are motivated by weighted Poincaré estimates that arise in the proofs of L^2 approximation property of the coarse interpolation in the analysis of domain decomposition preconditioners. In particular, the spectrum of local eigenvalue problem contains eigenvalues that are small and asymptotically vanish as the contrast increases. The eigenvectors corresponding to these small, asymptotically vanishing, eigenvalues represent the high-conducting features. The number of these eigenvectors is the same as the number of disconnected high-contrast inclusions. The coarse space is constructed such that the basis functions span the eigenfunctions corresponding to these small, asymptotically vanishing, eigenvalues as well as some nodal multiscale basis functions. In [18], we prove that if the coarse space in domain decomposition methods includes these eigenfunctions, then the condition number of the preconditioned matrix is bounded independent of the contrast.

In this paper, we use multiscale finite element framework and project the solution onto the coarse spaces obtained from local eigenvalue problem. As we mentioned that the eigenvectors represent high-conducting regions, and, consequently, multiscale basis functions represent high-conducting regions more accurately. However, for the accuracy of multiscale methods one also needs to

represent the fine-scale features of the solution away from these regions. Some of these features one can observe in eigenvectors that correspond to eigenvalues which are not asymptotically small. To capture these regions to some extend, we solve local problems subject to boundary conditions that come from the eigenvalue problem. As it was shown in [23, 14], the error in MsFEMs can be large when the coarse mesh size is close to a characteristic length scale for the coefficients with bounded variations. Thus, MsFEMs with proposed basis functions contain such resonance or residual error. In [12], the authors propose multiscale basis functions for high-contrast heterogeneities for problems with isolated inclusions where resonance errors are removed by carefully selecting boundary conditions. In [7], the authors propose global basis functions based on eigenvalue problems to remove these resonance errors.

In the paper, we compare MsFEM with local spectral basis functions with MsFEM that uses linear boundary conditions as well as energy minimizing basis functions. Our numerical results show that one can obtain more accurate solutions when local spectral basis functions are used. In particular, the high-conductivity features are captured more precisely with local spectral basis functions. These basis functions identify high-conductivity regions and are capable of separating them. Thus, the computed multiscale solutions capture high-conductivity regions. However, these basis functions still introduce errors due to the variations within high-conductivity regions and at the interfaces between high and low conductivity regions. More information is needed to incorporate these features into the basis functions. We discuss the use of global eigenvalue problem and the computation of it via local solutions. We propose the approximation of the global eigenvectors on a coarse grid using local spectral basis functions. We show that the number of small, asymptotically vanishing, eigenvectors remains the same in this approximation.

The paper is organized as follows. In the next section, we discuss domain decomposition and multiscale finite element frameworks. Section 3 is devoted to the discussion on coarse spaces. Numerical results are presented in Section 4. The use of global eigenvectors in multiscale simulations, their hierarchical approximations, and related numerical results are presented in Appendix.

2 Preliminaries. Domain decomposition and multiscale finite element methods

In this section, we describe domain decomposition and MsFEMs. These methods share similarities, though there are important differences. In particular, MsFEMs, as upscaling methods, compute the coarse-scale solution by using multiscale basis functions. Domain decomposition methods, on the other hand, use the information on the coarse grid and iteratively solve for the fine-scale solution by correcting its approximation at each iteration.

Let $D \subset \mathbb{R}^2$ (or $\mathbb{R}^3$) be a polygonal domain which is the union of a disjoint polygonal subregions $\{D_i\}_{i=1}^N$, called coarse grid. We consider the elliptic

equation with heterogeneous coefficients

$$div(\kappa(x)\nabla u) = f, \tag{1}$$

where $\kappa(x)$ is a heterogeneous field with high contrast. The variational formulation of this problem is

$$a(u,v) = f(v) \quad \text{for all } v \in H_0^1(D). \tag{2}$$

Here the bilinear form a and the linear functional f are defined by

$$a(u,v) = \int_D \kappa(x)\nabla u(x)\nabla v(x)dx \quad \text{for all } u,v \in H_0^1(D) \tag{3}$$

and

$$f(v) = \int_D f(x)v(x)dx \quad \text{for all } v \in H_0^1(D).$$

We assume $H = \max_i \operatorname{diam}(D_i)$. These coarse grids will be also denoted by $\mathcal{T}^H$. Let $\mathcal{T}^h$ be a fine triangulation which is a refinement of $\mathcal{T}^H$. We denote by $V^h(D)$ the usual finite element discretization of piecewise linear continuous functions with respect to the fine triangulation $\mathcal{T}^h$. Denote also by $V_0^h(D)$ the subset of $V^h(D)$ with vanishing values on ∂D. Similar notations, $V^h(\Omega)$ and $V_0^h(\Omega)$, are used for subdomains $\Omega \subset D$.

The Galerkin formulation of (2) is to find $u \in V_0^h(D)$ such that

$$a(u,v) = f(v) \quad \text{for all } v \in V_0^h(D), \tag{4}$$

or in matrix form

$$Au = b \tag{5}$$

where for all $u, v \in V^h(D)$ we have

$$u^T Av = \int_D \kappa\nabla u\nabla v \quad \text{and} \quad v^T b = \int_D fv.$$

We denote by $\{D_i'\}_{i=1}^N$ the overlapping decomposition obtained from the original nonoverlapping decomposition $\{D_i\}_{i=1}^N$ by enlarging each subdomain D_i to

$$D_i' = D_i \cup \{x \in D, \operatorname{dist}(x, D_i) < \delta_i\}, \quad i = 1, \ldots, N,$$

where dist is some distance function and let $V_0^i(D_i')$ be the set of finite element functions with support in D_i'. We also denote by $R_i^T : V_0^i(D_i') \to V^h$ the extension by zero operator.

Using the coarse interpolation $\mathcal{T}^H$ we introduce coarse basis functions $\{\Phi_i\}_{i=1}^{N_c}$ where N_c is the number of coarse mesh vertices. MsFEMs solve the underlying fine-scale equations on the coarse grid. Given coarse-scale basis functions the coarse space is given by

$$V_0 = \operatorname{span}\{\Phi_i\}_{i=1}^{N_c}, \tag{6}$$

and the coarse matrix $A_0 = R_0 A R_0^T$ where

$$R_0^T = [\Phi_1, \ldots, \Phi_{N_c}].$$

Multiscale finite element solution is the finite element projection of the fine-scale solution into the space V_0. More precisely, multiscale solution u_0 is given by

$$A_0 u_0 = f_0,$$

where $f_0 = R_0^T b$. One can also write the approximation on the coarse grid as $u_0 = \sum_i c_i \Phi_i$, where c_i are determined from

$$a(u_0, v) = (f, v), \quad \text{for all } v \in V_0.$$

Once u_0 is determined, one can define a fine-scale approximation of the solution by reconstructing via basis functions.

For domain decomposition methods, we use a two level additive preconditioner of the form

$$B^{-1} = R_0^T A_0^{-1} R_0 + \sum_{i=1}^{N} R_i^T A_i^{-1} R_i \tag{7}$$

where the local matrices are defined by

$$v A_i w = a(v, w) \quad \text{for all } v, w \in V_0^i(D_i'), \tag{8}$$

$i = 1, \ldots, N$. See [27, 22]. This procedure involves solving coarse-scale system and solving local problems in an iterative manner. This procedure involves solving coarse-scale system and local problems at each iteration. Each of the iteration can be used within an existing iterative methods, e.g., conjugate gradient, to converge to the fine-scale solution. In domain decomposition methods, a main goal is to reduce the number of iterations in the iterative procedure, while in multiscale methods, we would like to obtain an accurate approximation of the solution in a first iteration.

We denote by $\{y_i\}_{i=1}^{N_c}$ the vertices of the coarse mesh $\mathcal{T}^H$ and define the neighborhood of the node y_i by

$$\omega_i = \bigcup \{K_j \in \mathcal{T}^H; \quad y_i \in \overline{K}_j\} \tag{9}$$

and the neighborhood of the coarse element K by

$$\omega_K = \bigcup \{\omega_j \in \mathcal{T}^H; \quad y_j \in \overline{K}_j\}. \tag{10}$$

3 Coarse space

As we mentioned previously that both MsFEMs and domain decomposition methods use coarse spaces. In domain decomposition methods, one can do the simulations without the coarse space; however, as it has been shown that the

coarse spaces improve the convergence to a number of iterations independent of H and independent of the contrast for some special cases (see e.g., [22]). In this section we define local spectral multiscale coarse space using eigenvectors of high contrast eigenvalue problems. These multiscale basis functions are designed to improve the accuracy of multiscale methods for high-contrast problems. First, we define some notations.

To define the coarse space, we introduce high-contrast eigenvalue problem. For any $\Omega \subset D$ define the Neumann matrix A^{Ω} by

$$vA^{\Omega}w = \int_{\Omega} \kappa \nabla v \nabla w \quad \text{for all } v, w \in V^h(\Omega), \quad i = 1, \ldots, N, \tag{11}$$

and the mass matrix of same dimension M^{Ω} by

$$vM^{\Omega}w = \int_{\Omega} \kappa v w \quad \text{for all } v, w \in V^h(\Omega). \tag{12}$$

We consider the finite dimensional symmetric eigenvalue problem

$$A^{\Omega}\phi = \lambda M^{\Omega}\phi \tag{13}$$

and denote its eigenvalues and eigenvectors by $\{\lambda_{\ell}^{\Omega}\}$ and $\{\psi_{\ell}^{\Omega}\}$, respectively. Note that the eigenvectors $\{\psi_{\ell}^{\Omega}\}$ form an orthonormal basis of $V^h(\Omega)$ with respect to the M^{Ω} inner product. Note that $\lambda_1^{\Omega} = 0$. We assume that

$$\lambda_1^{\Omega} \leq \lambda_2^{\Omega} \leq \cdots \leq \lambda_i^{\Omega} \leq \ldots. \tag{14}$$

The eigenvalue problem above corresponds to the approximation of the eigenvalue problem

$$\operatorname{div}(\kappa \nabla v) = \lambda \kappa v$$

in Ω with Neumann boundary condition. In particular, $\psi_{\ell}^{\omega_i}$ denotes the ℓ-th eigenvector of the Neumann matrix associated to the neighborhood of y_i. Next, we present simple numerical examples to discuss the eigenvalues of the high-contrast eigenvalue problem. It turns out if the domain has m high-contrast inclusions, then there are m small, asymptotically vanishing, eigenvalues. This can be shown using min-max principles. In Figure 1, we present an example where there are 2 inclusions and 2 channels. As we observe there are four small, asymptotically vanishing, eigenvalues (see Figure 1). In general, if there are m inclusions and channels, then one can observe m small, asymptotically vanishing, eigenvalues. The eigenvectors corresponding to these eigenvalues will be used to construct the coarse space V_0. If Dirichlet boundary conditions are imposed, then the small eigenvalues are due to interior inclusions (see Figure 2).

We choose the basis functions such that they span the eigenfunctions corresponding to small, asymptotically vanishing, eigenvalues. We note that $\{\omega_i\}_{y_i \in \mathcal{T}^H}$ is a covering of Ω. Let $\{\chi_i\}_{i=1}^{N_c}$ be a partition of unity subordinated to the covering $\{\omega_i\}$ such that $\chi_i \in V^h(D)$ and $|\nabla \chi_i| \leq \frac{1}{H}$, $i = 1, \ldots, N_c$. Define the set of coarse basis functions

$$\Phi_{i,\ell} = I^h(\chi_i \psi_{\ell}^{\omega_i}) \quad \text{for } 1 \leq i \leq N_c \text{ and } 1 \leq \ell \leq L_i \tag{15}$$

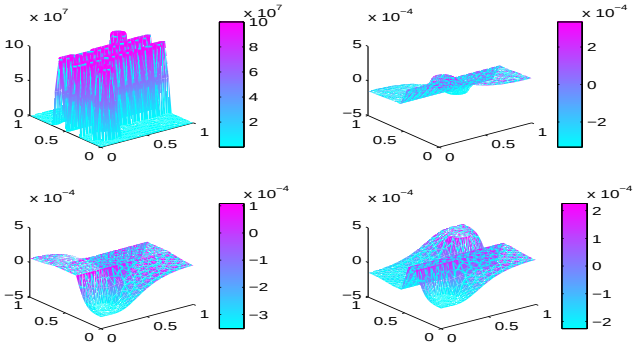

Figure 1: Eigenfunctions for Neumann problem. Permeability is 10^8 in the inclusions and channels and 1 outside. Left top: permeability. Right top: second eigenfunction (fist eigenfunction is constant). Left bottom: third eigenfunction. Right bottom: fourth eigenfunction. The four small eigenvalues are 0, $0.1119e-5$, $0.2409e-5$, $0.3310e-5$

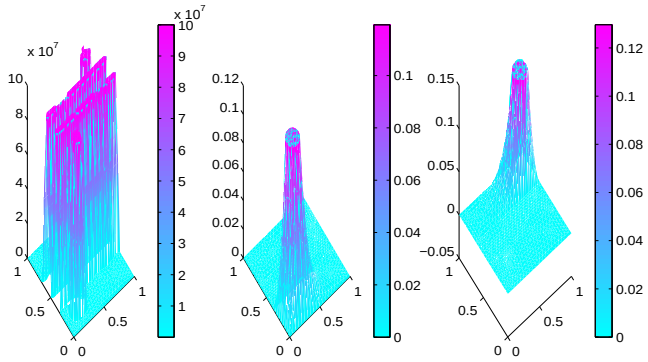

Figure 2: Eigenfunctions for Dirichlet problem with the same permeability as in Figure 1. Left: first eigenfunction. Right: second eigenfunction. The two small eigenvalues are $0.2922e-5$, $0.3183e-4$.

where L_i is an integer number for each $i = 1, \ldots, N_c$. Denote by V_0 the *local spectral multiscale* space

$$V_0 = \text{span}\{\Phi_{i,\ell} : 1 \leq i \leq N_c \text{ and } 1 \leq \ell \leq L_i\}. \tag{16}$$

Define also the coarse interpolation $I_0 : V \to V_0$ by

$$I_0 v = \sum_{i=1}^{N_c} \sum_{\ell=1}^{L_i} \left(\int_{\omega_i} \kappa v \psi_\ell^{\omega_i} \right) I^h(\chi_i \psi_\ell^{\omega_i}) = \sum_{i=1}^{N_c} I^h \left((I_{L_i}^{\omega_i} v) \chi_i \right), \tag{17}$$

where I^h is the fine-scale nodal value interpolation and $I_{L_i}^{\omega_i}$ was defined by

$$I_L^\Omega v = \sum_{\ell=1}^{L} \left(\int_\Omega \kappa v \psi_\ell^\Omega \right) \psi_\ell^\Omega. \tag{18}$$

Note that we have

$$v - I_0 v = \sum_{i=1}^{N_c} I^h \left(\chi_i (v - I_{L_i}^{\omega_i} v) \right).$$

We have the following weighted L^2 approximation and weighted H^1 stability properties ([18]).

Lemma 1 *For all coarse element K we have*

$$\int_K \kappa (v - I_0 v)^2 \preceq \frac{1}{\lambda_{K,L+1}} \int_{\omega_K} \kappa |\nabla v|^2 \tag{19}$$

$$\int_K \kappa |\nabla I_0 v|^2 \preceq \max\{1, \frac{1}{H^2 \lambda_{K,L+1}}\} \int_{\omega_K} \kappa |\nabla v|^2 \tag{20}$$

where $\lambda_{K,L+1} = \min_{y_i \in K} \lambda_{L_i+1}^{\omega_i}$ and ω_K is the union of the elements that share common edge with K defined in (10).

Lemma 1 allows us to show that the condition number of the preconditioned matrix is independent of contrast. In [18], we show that if the coarse space is the local spectral multiscale space as introduced in (16), then the condition number of the preconditioned matrix is independent of the contrast. In particular, the following lemma was proved in [18].

Lemma 2 *For all $v \in V^h$, there exists a decomposition $v = \sum_{i=0}^{N} v_i$, with $v_i \in V^i = V_0^h(D_i')$, $i = 1, 2, \ldots, N$, $v_0 \in V_0$, such that*

$$a(v_0, v_0) + \sum_{i=1}^{N} a(v_i, v_i) \preceq C_0^2 a(v, v)$$

with $C_0^2 \preceq \max\{1 + \frac{1}{\delta^2 \lambda_{L+1}}, 1 + \frac{1}{H^2 \lambda_{L+1}}\}$ where $\lambda_{L+1} = \min\limits_{1 \leq i \leq N_c} \lambda_{L_i+1}^{\omega_i}$.

As a corollary, we have the following statement.

Corollary 3 *Under the assumptions of Lemma 2 the condition number of the preconditioned operator $B^{-1}A$ with B^{-1} defined in (7) is*

$$cond(B^{-1}A) \preceq C(1 + \frac{H^2}{\delta^2})$$

where C is independent of the contrast and the mesh size.

3.1 Dimension reduction for the coarse space

As the high-contrast eigenvalue problem suggests that one can have a large number of basis functions if the number of separate high-contrast regions is large. This will result to a large dimensional coarse space. It is known when inclusions are strictly inside, one can use multiscale finite element basis functions for constructing the coarse space. One can reduce the dimension of the coarse space by identifying the basis functions with bounded energies. This procedure is presented in [18] and we will briefly outline it.

Previously, we used general partition of unity functions. One can use the partition of unity functions $\{\chi_i\}_{i=1}^{N_c}$ that provide the least energy. This can be accomplished by solving

$$\min \sum_{i=1}^{N_c}\sum_{\ell=1}^{L_i}\int_{\omega_i}\kappa|\nabla\Phi_{i,\ell}|^2 = \sum_{i=1}^{N_c}\sum_{\ell=1}^{L_i}\int_{\omega_i}\kappa|\nabla(\chi_i\psi_\ell^{\omega_i})|^2 \tag{21}$$

where the local spectral multiscale basis functions $\Phi_{i,\ell}$ are defined in (15) and the minimum is taken over all partition of unity functions $\{\chi_i\}_{i=1}^{N_c}$ subordinated to the covering $\{\omega_i\}_{i=1}^{N_c}$ of D. One can solve (21) following the similar procedure as discussed in [29].

The numerical solution of the energy minimizing problem (21) is computationally expensive since it involves computing a global problem. One can use instead multiscale basis functions that reduce the energy of the basis functions defined via eigenfunctions. Following [17], we define the *local spectral multiscale basis functions with reduced energy* $\widetilde{\Phi}_{i,\ell}$ as the $\kappa-$harmonic extension of $\Phi_{i,\ell}$ in each coarse block, that is, for each coarse element K and $1 \leq \ell \leq L_i$ with $1 \leq i \leq N_c$ we have

$$\begin{aligned} div(\kappa\nabla\widetilde{\Phi}_{i,\ell}) &= 0 \quad \text{in } K \\ \widetilde{\Phi}_{i,\ell} &= \Phi_{i,\ell} \quad \text{on } \partial K. \end{aligned} \tag{22}$$

We define *local spectral multiscale coarse space with reduced energy* by

$$V_0 = \text{span}\{\widetilde{\Phi}_i\}_{i=1}^{N_c}. \tag{23}$$

These basis functions are only used to reduce the dimension of the coarse space by removing those basis functions with bounded energy. We also define standard

multiscale finite element basis functions (as defined in [23]). In this case, we only choose the constant eigenfunction and thus have only one function per node defined as

$$\begin{aligned} div(\kappa\nabla\widetilde{\Phi}_i) &= 0 \quad \text{in } K \\ \widetilde{\Phi}_i &= \chi_i \quad \text{on } \partial K. \end{aligned} \tag{24}$$

The standard multiscale basis functions are defined by

$$V_0^{ms-lin} = \text{span}\{\widetilde{\Phi}_i\}_{i=1}^{N_c}. \tag{25}$$

Energy minimizing nodal basis functions are defined by taking only the constant eigenfunction in (21), i.e.,

$$\min \sum_{i=1}^{N_c} \sum_{\ell=1}^{L_i} \int_{\omega_i} \kappa |\nabla \Phi_i|^2 \tag{26}$$

and we denote the span of these basis functions by V_0^{EM}.

Our motivation for the reduction stems from the fact that when high-contrast inclusions are isolated and away from the boundaries of coarse-grid blocks, the energies of the basis functions are bounded unlike the energies of the basis functions corresponding to channels. For this reason, we perform local singular value decomposition and isolate the basis functions that represent high-conductivity channels from basis functions that represent the inclusions with bounded energy. The approach is as follows. Given a coarse mesh node y_i we consider the space spanned by all the coarse basis functions associated to this node. Then divide this space according to the energy, keeping the part of the space with higher energy. More precisely, consider the L_i basis functions associated to this node, that is

$$\Phi_{i,\ell}, \text{ with } 1 \leq \ell \leq L_i$$

and define the matrix

$$R_0^{iT} = [\Phi_{i,1}, \ldots, \Phi_{i,L_i}].$$

We have that the coarse space spanned by multiscale basis functions (see (16)) can be written as $V_0 = \text{span}_{1\leq i\leq N_c} R_0^{iT}$. We define the local coarse matrix of dimension $L_i \times L_i$ by

$$A_0^i = R_0^{iT} A R_0^i.$$

In the case of V_0 defined by (23) the basis functions $\Phi_{i,1}$ are usual multiscale basis functions with linear boundary conditions. We write the eigenvalue decomposition of this symmetric matrix as

$$A_0^i = Q_0^{Ti} D_0^i Q_0^i, \quad Q_0^i = [q_{i,1}, \ldots, q_{i,L_i}] \tag{27}$$

where the matrix Q_0^i is an orthogonal matrix and $D_0^i = \text{diag}(\mu_1, \ldots, \mu_{L_i})$ with

$$\mu_1 \leq \cdots \leq \mu_{L_i}.$$

The idea is to keep only the part of span$\{R_0^{iT}\}$ associated with larger energy. To do this we remove the first M_i eigenvectors in (27) that have bounded energies independent of the contrast. In case of interior high-contrast inclusions and channels, M_i can be chosen as the number of small, asymptotically vanishing, eigenvalues corresponding to the zero Dirichlet local high-contrast eigenvalue problem. Define the matrix of eigenvalues of larger energy by

$$\widehat{Q}_0^i = [0, \ldots, 0, q_{i,M_i+1} \ldots, q_{i,L_i}].$$

The new basis functions associated to the coarse mesh node y_i will be given by the columns of the matrix $R_0^i \widehat{Q}_0^i$ and the multiscale basis function $\Phi_{1,i}$ (or energy minimizing basis functions as defined in [20, 29]). We define the new reduced local spectral multiscale space

$$V_0 = \text{span}\{\Phi_{i,1}, R_0^i \widehat{Q}_0^i\}_{i=1}^{N_c}. \tag{28}$$

Note that one can determine the number of basis functions associated with interior inclusions by solving zero Dirichlet eigenvalue problem instead of zero Neumann problem. However, to identify the eigenvectors that represent channels is not easy because many eigenvectors have components in the channel regions. By using local spectral multiscale coarse space with reduced energy, our goal is to identify the basis corresponding to inclusions.

If isolated inclusions intersect the boundaries, multiscale finite element basis functions with linear boundary conditions can give large (contrast dependent) energies for such isolated inclusions. In [19], the authors construct multiscale basis functions with bounded energies for isolated high-contrast inclusions intersecting the boundary by using reduced one-dimensional boundary conditions. These boundary conditions provide more accurate representation of high-contrast features. These basis functions can be used to reduce the dimension of the coarse space defined by local spectral problem (as in (16)). In this case the basis functions with bounded energies will be replaced by energy minimizing basis functions as defined in [20].

4 Numerical studies

In this section, we present representative numerical results for MsFEMs and the additive preconditioner with the local spectral multiscale coarse spaces. In particular, we will use the following notations. LSM$_1$ will refer to multiscale or domain decomposition methods with local spectral multiscale coarse space as defined in (16), where the eigenvectors corresponding to small, asymptotically vanishing eigenvalues, are multiplied by piecewise linear partition of unity functions. LSM-RE will refer to multiscale or domain decomposition methods with local spectral multiscale coarse space as defined in (23), where we use basis functions with reduced energy. RLSM will refer to multiscale or domain decomposition methods with local spectral multiscale coarse space as defined in (28), where the coarse space dimension is reduced. We take $D = [0, 1] \times [0, 1]$ that is

divided into 10×10 equal square subdomains. Inside each subdomain we use a fine-scale triangulation where triangular elements constructed from 10×10 squares are used.

In our first numerical example, we use the coefficient depicted in Figure 3 that corresponds to a coefficient with background one and high conductivity channels and inclusions with varying conductivities within each region. In particular, we choose the high conductivities between $\eta/10$ and η randomly for each region. Here η is a fixed large number. In Figure 4, we depict fine-scale solution and the solution obtained with various coarse space for the coarse mesh size $H = 1/10$. In the title of the figures, the relative errors in energy norm as well as H^1 norm are shown. The errors are the following: the errors with multiscale basis functions obtained using local solutions with linear boundary conditions (see (25)) are 98.25% (in energy norm) and 97.9% (in H^1 norm); the errors with multiscale basis functions obtained using energy minimizing basis functions (see (26)) are 24.66% (in energy norm) and 24.9% (in H^1 norm); the errors with multiscale basis functions obtained using local spectral basis (see (16)) are 11.88% (in energy norm) and 11.88% (in H^1 norm); the errors with multiscale basis functions obtained using reduced local spectral basis (see (23)) are 6.11% (in energy norm) and 6.11% (in H^1 norm); the errors with multiscale basis functions obtained using local spectral basis with reduced dimension (see (28)) are 10% (in energy norm) and 10% (in H^1 norm). We observe that MsFEM with spectral basis functions perform better than other standard MsFEM methods. In particular, MsFEM with reduced energy basis gives the most accurate results. In Tables 1 and 2, we present the errors between the fine-scale solution and the multiscale solution in energy norm and weighted L^2 norm. The errors are shown for two different contrasts and two different coarse mesh sizes, $H = 1/10$ and $H = 1/20$. We observe from this table that the weighted L^2 norm are small for all the methods; however, the errors in energy norms can be large. In particular, multiscale basis functions with linear boundary conditions and energy minimizing basis functions give large errors. The errors are smallest for MsFEM with LSM-RE basis functions, though we observe that the error does not decrease as the mesh size is reduced and there is some residual error that MsFEM with spectral basis can not remove. In Figure 5, we depict logarithm of the square of the velocity field, $\kappa^2|\nabla p|^2$. It is evident from this figure that MsFEM with spectral basis functions capture the sharp features more accurately; however, it may not accurately capture the features that are smoother and away from sharp interfaces. To make MsFEM with spectral basis more accurate, one can include more basis elements that capture the features in low conductivity regions. For example, one can include eigenfunctions that correspond to eigenvalues that are not asymptotically small. In Table 3, we show the number of iterations for different methods with varying contrast. As we observe that domain decomposition methods that use spectral basis functions provide the least number of iterations and the condition number is bounded independent of the contrast.

In our second numerical example, we use the coefficient depicted in Figure 6 that corresponds to a coefficient with background one and high conductivity

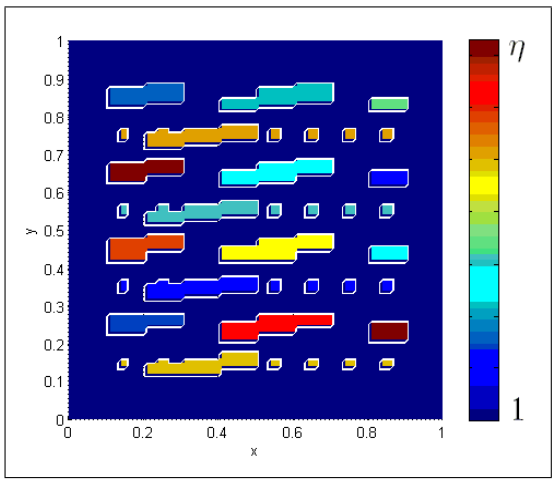

Figure 3: Permeability field.

H	MS	EMF	LSM_1	LSM-RE	RLSM
1/10	0.98(0.98)	0.24(0.24)	0.11(0.11)	0.06(0.06)	0.10(0.10)
1/20	1.46(1.47)	0.85(0.87)	0.14(0.14)	0.09(0.09)	0.13(0.13)

Table 1: Relative energy error for the permeability depicted in Figure 3. Here $h = 1/100$, $\eta = 10^4$ ($\eta = 10^6$).

channels and inclusions with varying conductivities within each region. In particular, we add a long channel in this example compared to the previous one. We choose the high conductivities between $\eta/10$ and η randomly for each region, where η is a fixed number. In Figure 7, we depict the fine-scale solution and the solution obtained with various coarse spaces for the coarse mesh $H = 1/10$. In the title of the figures, the relative errors in energy norm as well as H^1 norm are shown. The errors are the following: the errors with multiscale basis functions obtained using local solutions with linear boundary conditions (see (25)) are 68% (in energy norm) and 68% (in H^1 norm); the errors with multiscale basis functions obtained using energy minimizing basis functions (see (26)) are 24.45% (in energy norm) and 24.45% (in H^1 norm); the errors with multiscale basis functions obtained using local spectral basis (see (16)) are 18.19% (in energy norm) and 18.19% (in H^1 norm); the errors with multiscale basis functions obtained using reduced local spectral basis (see (23)) are 12.81% (in energy

H	MS	EMF	LSM_1	LSM-RE	RLSM
1/10	0.03(0.03)	0.001(0.001)	0.0003(0.0003)	0.0003(0.0003)	0.0002(0.0002)
1/20	0.06(0.07)	0.03(0.04)	0.00004(0.00006)	0.0001(0.0001)	0.0004(0.0003)

Table 2: Relative weighted L^2 error for the permeability depicted in Figure 3. Here $h = 1/100$, $\eta = 10^4$ ($\eta = 10^6$).

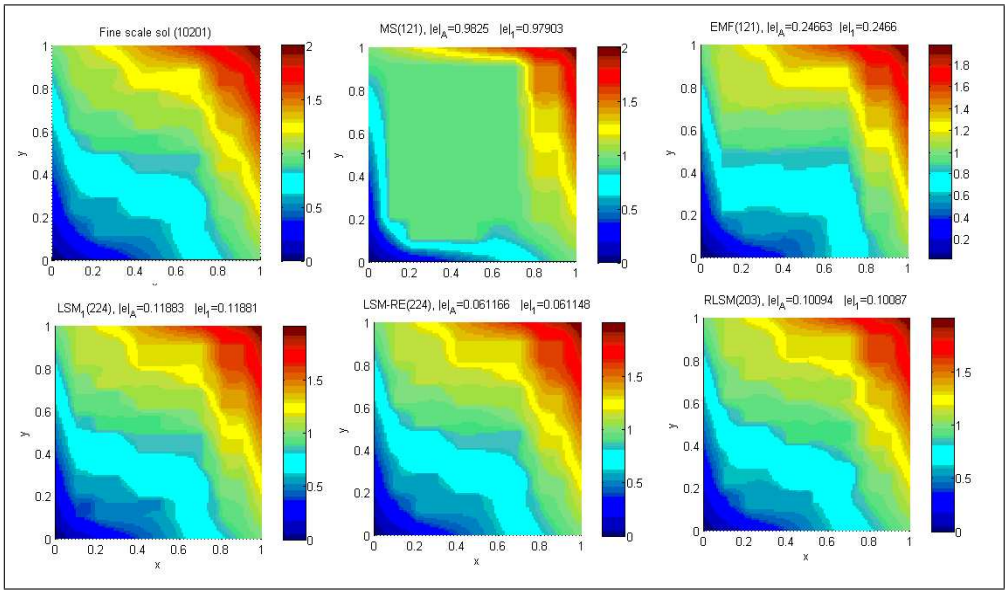

Figure 4: Multiscale finite element approximation on a coarse grid $H = 1/10$. In the title, the dimension of the coarse space is shown. $\eta = 10^4$.

η	MS	EMF	LSM_1	LSM-RE	RLSM
10^6	238(1.52e+006)	89(4.22e+002)	37(1.08e+001)	33(1.06e+001)	35(1.13e+001)
10^8	345(1.45e+008)	99(4.22e+002)	38(1.08e+001)	33(1.06e+001)	36(1.13e+001)
10^{10}	455(1.52e+010)	132(4.22e+002)	41(1.08e+001)	38(1.06e+001)	36(1.13e+001)

Table 3: Number of iterations until convergence of the PCG and condition number for different values of the contrast η with the coefficient in Figure 3. We set the tolerance to 1e-10. Here $H = 1/10$ with $h = 1/100$.

norm) and 12.81% (in H^1 norm); the errors with multiscale basis functions obtained using local spectral basis with reduced dimension (see (28)) are 15.84% (in energy norm) and 15.84% (in H^1 norm). Again, we observe that MsFEM with spectral basis functions perform better than other methods. In particular, MsFEM with reduced energy basis gives the most accurate results among the methods are considered. In Tables 4 and 5, we present the errors between the fine-scale solution and the multiscale solution in energy norm and weighted L^2 norm. The errors are shown for two different contrasts and two different coarse mesh sizes, $H = 1/10$ and $H = 1/20$. We observe that the weighted L^2 norm are small for all the methods; however, the errors in energy norms can be large. In particular, multiscale basis functions with linear boundary conditions and energy minimizing basis functions give large errors. Moreover, we note that MsFEM with local spectral basis functions is robust with respect to coarse mesh size and the contrast. We again observe that MsFEM with reduced energy basis gives the smallest error, though there is some residual error that is not removed.

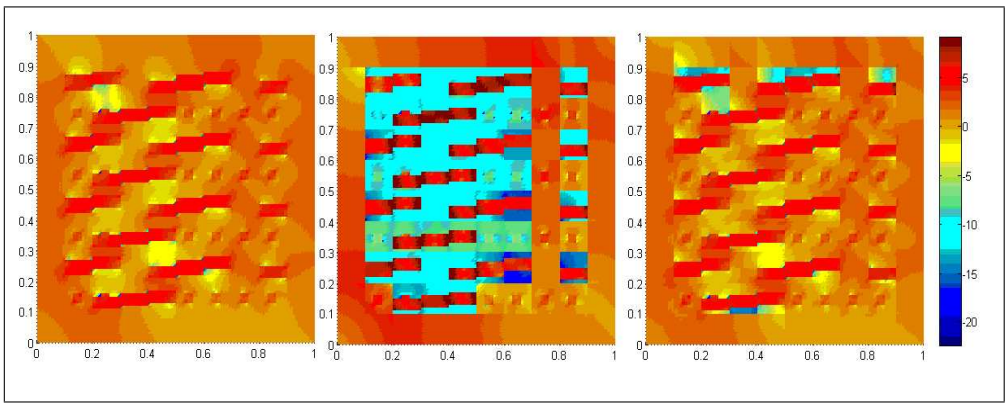

Figure 5: Logarithm of the velocity square ($\kappa^2|\nabla p|^2$) is depicted for the fine-scale solution (left), standard MsFEM with basis functions that have linear boundary conditions (middle), and MsFEM with reduced energy basis (right). This corresponds to the permeability field depicted in in Figure 3. $\eta = 10^6$

In Table 6, we show the number of iterations for different methods with varying contrast. As we observe that domain decomposition methods that use spectral basis functions provide the least number of iterations and the condition number is bounded independent of the contrast.

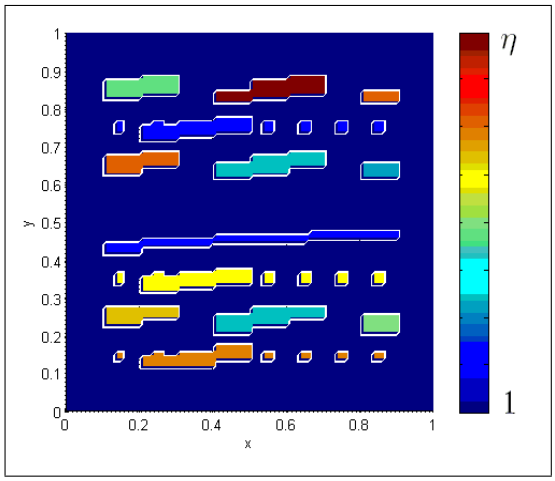

Figure 6: Permeability field.

In our third numerical example, we use the coefficient depicted in Figure 8 that corresponds to a coefficient with background one and high conductivity channels and inclusions with varying conductivities within each region. In particular, we add a long tortuous channel in this example compared to the previous one. We choose the high conductivities between $\eta/10$ and η randomly

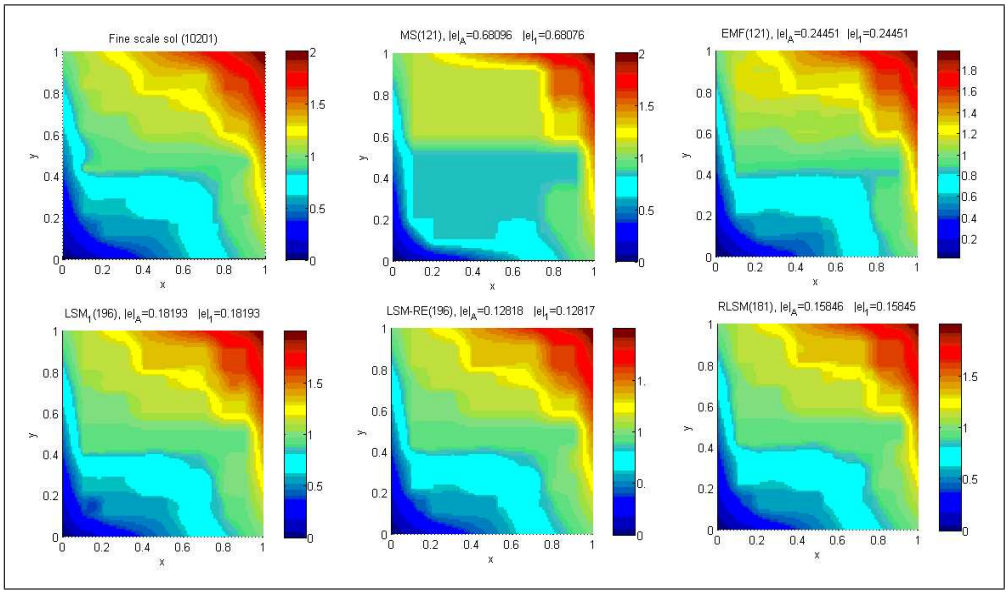

Figure 7: Multiscale finite element approximation on a coarse grid $H = 1/10$. In the title, the dimension of the coarse space is shown. $\eta = 10^5$.

H	MS	EMF	LSM_1	LSM-RE	RLSM
1/10	0.67(0.68)	0.24(0.24)	0.18(0.18)	0.12(0.12)	0.15(0.15)
1/20	0.84(0.84)	0.55(0.56)	0.17(0.17)	0.12(0.13)	0.15(0.15)

Table 4: Relative energy error for the permeability depicted in Figure 6. Here $h = 1/100$, $\eta = 10^5$ ($\eta = 10^7$).

for each region. In Figure 9, we depict fine-scale solution and the solution obtained with various coarse spaces. In the title of the figures, the relative errors in energy norm as well as H^1 norm are shown. The errors are the following: the errors with multiscale basis functions obtained using local solutions with linear boundary conditions (see (25)) are 68% (in energy norm) and 68% (in H^1 norm); the errors with multiscale basis functions obtained using energy minimizing basis functions (see (26)) are 24.45% (in energy norm) and 24.45% (in H^1 norm); the errors with multiscale basis functions obtained using local spectral basis (see (16)) are 18.19% (in energy norm) and 18.19% (in H^1 norm); the

H	MS	EMF	LSM_1	LSM-RE	RLSM
1/10	0.02(0.02)	0.001(0.001)	0.0003(0.0003)	0.0003(0.0003)	0.0003(0.0003)
1/20	0.03(0.03)	0.02(0.02)	0.0001(0.0001)	0.0002(0.0002)	0.0003(0.0003)

Table 5: Relative weighted L^2 error for the permeability depicted in Figure 6. Here $h = 1/100$, $\eta = 10^5$ ($\eta = 10^7$).

η	MS	EMF	LSM_1	LSM-RE	RLSM
10^6	141(1.07e+005)	78(1.17e+002)	37(1.11e+001)	36(1.09e+001)	39(1.14e+001)
10^8	141(1.07e+005)	78(1.17e+002)	37(1.11e+001)	36(1.09e+001)	39(1.14e+001)
10^{10}	141(1.07e+005)	78(1.17e+002)	37(1.11e+001)	36(1.09e+001)	39(1.14e+001)

Table 6: Number of iterations until convergence of the PCG and condition number for different values of the contrast η with the coefficient in Figure 6. We set the tolerance to 1e-10. Here $H = 1/10$ with $h = 1/100$.

errors with multiscale basis functions obtained using reduced local spectral basis (see (23)) are 12.81% (in energy norm) and 12.81% (in H^1 norm); the errors with multiscale basis functions obtained using local spectral basis with reduced dimension (see (28)) are 15.84% (in energy norm) and 15.84% (in H^1 norm). Again, we observe that MsFEM with spectral basis functions perform better than other methods. In particular, MsFEM with reduced energy basis gives the most accurate results among the methods are considered. In Tables 7 and 8, we present the errors between the fine-scale solution and the multiscale solution in energy norm and weighted L^2 norm. The errors are shown for two different contrasts and two different coarse mesh sizes, $H = 1/10$ and $H = 1/20$. We observe from this table that the weighted L^2 norm are small for all the methods; however, the errors in energy norms can be large. In particular, multiscale basis functions with linear boundary conditions and energy minimizing basis functions give large errors. Moreover, we note that MsFEM with local spectral basis functions is robust with respect to coarse mesh size and the contrast. We again observe that MsFEM with reduced energy basis gives the smallest error. In Table 9, we show the number of iterations for different methods with varying contrast. As we observe that domain decomposition methods that use spectral basis functions provide the least number of iterations and the condition number is bounded independent of the contrast.

H	MS	EMF	LSM_1	LSM-RE	RLSM
1/10	0.72(0.73)	0.38(0.56)	0.23(0.23)	0.09(0.09)	0.13(0.13)
1/20	0.57(0.58)	0.40(0.42)	0.19(0.19)	0.12(0.12)	0.12(0.12)

Table 7: Relative energy error for the permeability field depicted in Figure 8. Here $h = 1/100$, $\eta = 10^4$ ($\eta = 10^6$).

H	MS	EMF	LSM_1	LSM-RE	RLSM
1/10	0.03(0.03)	0.004(0.01)	0.0006(0.0006)	0.0002(0.0002)	0.0003(0.0003)
1/20	0.03(0.03)	0.01(0.01)	0.0005(0.0005)	0.00003(0.00003)	0.00005(0.00005)

Table 8: Relative weighted L^2 error for the permeability field depicted in Figure 8. Here $h = 1/100$, $\eta = 10^5$ ($\eta = 10^7$).

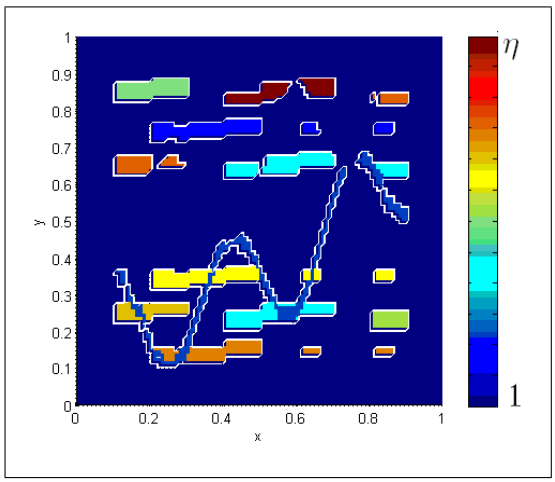

Figure 8: Permeability field

η	MS	EMF	LSM_1	LSM-RE	RLSM
10^6	175(3.30e+005)	77(1.25e+003)	44(1.56e+001)	37(1.19e+001)	39(1.19e+001)
10^8	260(3.30e+007)	127(1.21e+005)	47(1.56e+001)	40(1.19e+001)	41(1.19e+001)
10^{10}	455(1.52e+010)	132(4.22e+002)	41(1.08e+001)	38(1.06e+001)	36(1.13e+001)

Table 9: Number of iterations until convergence of the PCG and condition number for different values of the contrast η with the coefficient in Figure 8. We set the tolerance to 1e-10. Here $H = 1/10$ with $h = 1/100$.

4.1 Discussions

Above numerical results show that MsFEMs with local spectral basis functions can capture the high-conductivity features of the solution more accurately; however, they do not necessarily provide an accurate approximation of the solution. In particular, the fine-scale behavior of the solution representing the interaction of high-conductivity regions may not be accurately captured with these basis functions. To discuss it further, we consider discrete spectral representation of the fine-scale equation (see (5))

$$Au = b.$$

It is known that the matrix A can be written as

$$A = \sum_{i=1}^{N} \lambda_i (M\phi_i)(M\phi_i)^T,$$

where N is the total number of eigenvectors of

$$A\phi_i = \lambda_i M\phi_i$$

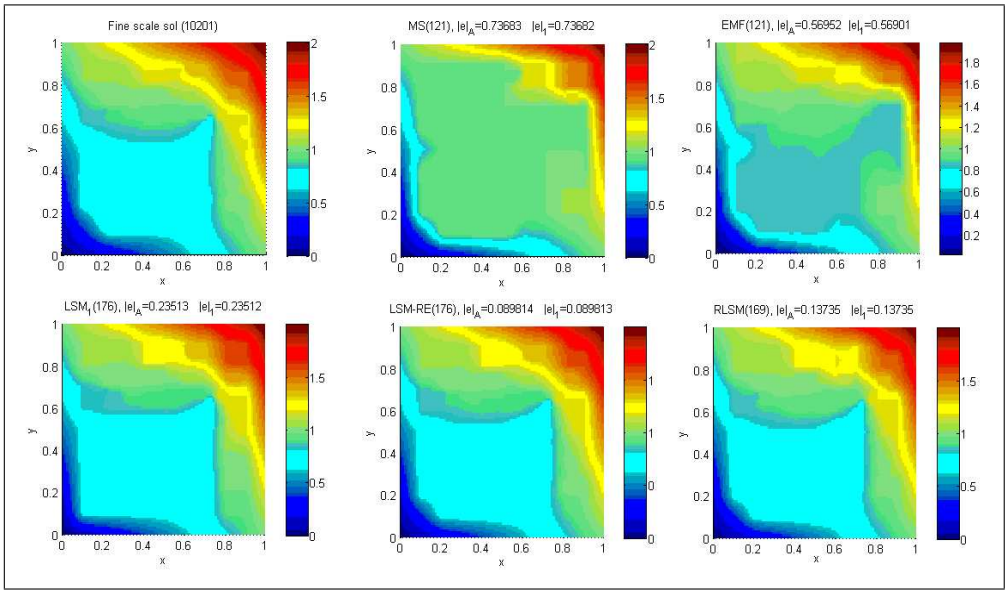

Figure 9: Multiscale finite element approximation on a coarse grid $H = 1/10$. In the title, the dimension of the coarse space is shown. $\eta = 10^6$.

defined by (13). Similarly, we define

$$A_0 = \sum_{i=1}^{L} \lambda_i (M\phi_i)(M\phi_i)^T,$$

where λ_1, ..., λ_L are asymptotically vanishing eigenvalues. Note that we consider the global eigenvalue problem here. In general, we have observed that one can approximate global eigenvectors hierarchically by using local spectral basis functions. This is because local eigenvectors corresponding to small, asymptotically vanishing eigenvalues capture the high conductivity features of the solution. In Appendix A, we include a discussion on computing global eigenvectors via local ones and numerical results. We note that the number of small, asymptotically vanishing, eigenvalues remain the same when local basis functions are used. This can be easily verified. The approximation of the eigenvectors is accurate as we observe in our simulations because local spectral basis functions contain high-contrast features and are capable representing them on a larger scale.

We denote

$$\hat{A} = A - A_0 = \sum_{i=L+1}^{N} \lambda_i (M\phi_i)(M\phi_i)^T.$$

Similarly,

$$u_0 = \sum_{i=1}^{L} (u, M\phi_i)\phi_i, \quad \hat{u} = \sum_{i=L+1}^{N} (u, M\phi_i)\phi_i,$$

such that

$$A_0 u_0 = b_0, \quad \hat{A}\hat{u} = \hat{b}.$$

Multiscale basis functions introduced above span the eigenfunctions corresponding to asymptotically vanishing eigenvalues. These basis functions also span χ_j that represent partition of unity functions. The eigenfunctions ψ_l are designed to capture the high-conducting regions, while χ_j can be regarded as basis functions for approximating the solution of the equation $\hat{A}\hat{u} = \hat{b}$. This equation is independent of the contrast and we use standard multiscale techniques for approximating its solution. It is possible that one needs more information to capture the fine-scale details of the solution. In this case, more basis functions χ_j can be taken or some limited global information can be used in computing χ_j.

5 Conclusions

In this paper, we studied MsFEMs using basis functions that provide optimal convergence in domain decomposition methods. These basis functions are designed to capture high-conducting regions in the solution. Both multiscale finite element and domain decomposition methods (considered here) use coarse spaces to achieve efficiency and robustness. In MsFEMs, the spatial variability of the media affects the convergence rate. In domain decomposition methods, high variability of the coefficients within coarse regions affects the number of iterations required for the convergence, and thus it is important to represent these features in the coarse space. While in MsFEMs, one needs also to represent the fine-scale behavior of the solution away from high-conducting regions. In this paper, we used coarse spaces designed for high-contrast problems that provide an optimal convergence in domain decomposition methods. In particular, basis functions are constructed using solutions of a local spectral problem. In our previous work [18], we show that using these coarse spaces one can construct preconditioners such that the condition number of the preconditioned system is independent of the contrast. In this paper, these coarse spaces are used in MsFEMs to solve elliptic equations with high-contrast heterogeneous coefficients on a coarse grid. Our numerical results show that MsFEMs with coarse spaces constructed via local spectral problems are more accurate compared to multiscale methods that employ traditional multiscale spaces with linear boundary conditions. However, these basis functions may not accurately capture the features of the solution within high-conducting regions or outside. As a result, some residual error remains that can not be removed by MsFEM with local spectral basis functions. One can lower the error by adding additional basis functions, for example, using eigenvectors that correspond to eigenvalues that are not asymptotically small. This is a subject of future research. In this paper, we also discuss hierarchical approximation of the basis functions that provides CPU savings when using large coarse grids. The numerical results are presented for both MsFEMs and domain decomposition methods for the sake of completeness. We consider several basis functions. We show that the basis functions

with reduced energy that uses local spectral information provides the smallest error in the energy norm. These basis functions use the information on the boundaries and solves the local problems within the region. We observe that MsFEMs with standard and energy minimizing basis functions give large errors.

6 Acknowledgments

The work of YE and JG is partially supported by Award Number KUS-C1-016-04, made by King Abdullah University of Science and Technology (KAUST). YE's work is partially supported by NSF and DOE.

A Global eigenvectors and their hierarchical approximations

In general, it is not clear that one can obtain accurate multiscale approximation with local basis functions (see [7]). In [7], the authors use eigenvectors of special eigenvalue problem to show the convergence independent of contrast. Here, we use eigenvectors of weighted eigenvalue problem and obtain convergence results. The computations of the eigenvectors are expensive and thus hierarchical computations are needed.

Consider a global homogeneous Neumann problem in D for

$$div(\kappa(x)\nabla u) = f. \tag{29}$$

Define the global eigenvalue problem with homogeneous Neumann boundary conditions

$$div(\kappa(x)\nabla\phi_i^g) = \lambda_i^g \kappa\nabla\phi_i^g.$$

It can be shown that for any v

$$v = \sum \alpha_i^g(v)\phi_i^g,$$

where

$$\alpha_i^g(v) = \int_D kv\phi_i^g = \frac{1}{\lambda_i^g}\int_D k\nabla v\nabla\phi_i^g.$$

Multiplying both sides of (29) by ϕ_i^g and integrating over D, we have

$$\int_D \kappa\nabla u\nabla\phi_i^g = \int_D f\phi_i^g.$$

Consequently,

$$\alpha_i^g(u) = \frac{1}{\lambda_i^g}\int_D f\phi_i^g \leq \frac{1}{\lambda_i^g}(\int_D \kappa^{-1}f^2)^{1/2}.$$

If multiscale basis functions span ϕ_1^g, ..., ϕ_L^g (eigenvectors corresponding to small, asymptotically vanishing, eigenvalues) then it can be shown that

$$\frac{\int_D \kappa|\nabla(u-u_0)|^2}{\int_D k|\nabla u|^2} = \frac{\sum_{i=L+1}^N \lambda_i^g(\alpha_i^g(u))^2}{\sum_{i=1}^N \lambda_i^g(\alpha_i^g(u))^2} \leq \frac{\sum_{i=L+1}^N 1/\lambda_i^g}{\sum_{i=1}^N 1/\lambda_i^g}. \tag{30}$$

From here, we see that the error is small provided that the right hand side of (30) is small. We have observed that if one places sources and sinks within the high-conducting regions, the approximation with leading order eigenvectors is very accurate. Here, leading order eigenvectors refer to those that correspond to small, asymptotically vanishing, eigenvalues. This approximation deteriotes if the source terms are placed outside high-conducting regions.

A.1 Hierarchical computations of basis functions

The computations of eigenvectors corresponding to small, asymptotically vanishing, eigenvectors can be expensive if the coarse grid contains many fine-grid blocks. In this case, one can compute the eigenvectors via hierarchical approaches as in multigrid methods. To demonstrate the main idea of this procedure, we consider the computation of an eigenvector, Ψ

$$div(\kappa\nabla\Psi) = \Lambda k\Psi \quad \text{in } \Omega_i, \tag{31}$$

where Λ is a small eigenvalue number in a larger domain and Ω_i is a larger coarse-grid block. We assume that Ω_i is divided into coarse-grid blocks ω_j and for each ω_j, the local eigenvectors corresponding to small, asymptotically vanishing, eigenvalues are used to solve for Ψ. Next, we present rigorous formulation of the hierarchical approximation.

A.1.1 Mathematical formulation

We introduce a triangulation $\mathcal{T}^{\widetilde{H}}$. We assume that $h < H < \widetilde{H}$. We also assume that $\mathcal{T}^h$ is a refinement of $\mathcal{T}^H$ which in turns is a refinement of $\mathcal{T}^{\widetilde{H}}$.

We denote by $\{\widetilde{z}_j\}_{j=1}^{\widetilde{N}_c}$ the vertices of the coarse mesh $\mathcal{T}^{\widetilde{H}}$ and define the neighborhood of the node $\widetilde{z}_j$ by

$$\widetilde{\omega}_j = \bigcup\{\widetilde{K} \in \mathcal{T}^{\widetilde{H}}; \quad \widetilde{z}_j \in \overline{\widetilde{K}}\} \tag{32}$$

and the neighborhood of the coarse element $\widetilde{K} \in \mathcal{T}^{\widetilde{H}}$ by

$$\widetilde{\omega}_{\widetilde{K}} = \bigcup\{\widetilde{\omega}_j; \quad \widetilde{z}_j \in \overline{\widetilde{K}}\}. \tag{33}$$

For each $j = 1, \ldots, \widetilde{N}_c$ we will restrict the coarse space V_0 defined in (16) to the coarse node neighborhood $\widetilde{\omega}_j$, that is, we define

$$V_0^{\widetilde{\omega}_j} = \text{span}\{I^h(\chi_i\psi_\ell^{\omega_i\cap\widetilde{\omega}_j}) : y_i \in \mathcal{T}^H, y_i \in \widetilde{\omega}_j \text{ and } 1 \leq \ell \leq L_i\}, \tag{34}$$

where the fine scale local eigenvector $\psi_\ell^{\omega_i\cap\widetilde{\omega}_j}$ was define in (13) and I^h is the fine-scale nodal value interpolation. Recall that if $y_i \in \mathcal{T}^H$ is a node interior to $\widetilde{\omega_j}$ we have $\omega_i \subset \widetilde{\omega}_j$. We define the local coarse matrices $A_0^{\widetilde{\omega}_j}$ and $M_0^{\widetilde{\omega}_j}$ by

$$A_0^{\widetilde{\omega}_j} = R_0^{\widetilde{\omega}_j} A R_0^{\widetilde{\omega}_j T} \text{ and } M_0 = R_0^{\widetilde{\omega}_j} M R_0^{\widetilde{\omega}_j T} \tag{35}$$

where $R_0^{\widetilde{\omega}_j T}$ is the matrix whose columns are the basis functions of $V_0^{\widetilde{\omega}_j}$ define in (34),

$$R_0^{\widetilde{\omega}_j T} = [I^h(\chi_i \psi_\ell^{\omega_i\cap\widetilde{\omega}_j})]_{y_i\in\widetilde{\omega}_j, 1\leq\ell\leq L_i}.$$

We denote by $\{\widetilde{\lambda}_m^{\widetilde{\omega}_j}\}$ and $\{\widetilde{\phi}_m^{\widetilde{\omega}_j}\}$ the increasing ordered eigenvalues and eigenvectors of the $\mathcal{T}^H-$coarse level eigenvalue problem in $\widetilde{\omega}_j$,

$$A_0^{\widetilde{\omega}_j}\widetilde{\phi}_m^{\widetilde{\omega}_j} = \widetilde{\lambda}_m^{\widetilde{\omega}_j} M_0^{\widetilde{\omega}_j}\widetilde{\phi}_m^{\widetilde{\omega}_j}.$$

Let $\{\widetilde{\chi}_j\}_{j=1}^{\widetilde{N}_c}$ be a partition of unity subordinated to the covering $\{\widetilde{\omega}_j\}$ such that $\widetilde{\chi}_j \in V^h$ and $|\nabla\widetilde{\chi}_j| \leq \frac{1}{\widetilde{H}}$, $j = 1, \ldots, \widetilde{N}_c$. Define the coarse basis functions

$$\widetilde{\Phi}_{j,m} = I^h(\chi_j(R_0^{\widetilde{\omega}_j}\widetilde{\phi}_m^{\widetilde{\omega}_j})) \quad \text{ for } 1 \leq j \leq \widetilde{N}_c \text{ and } 1 \leq m \leq \widetilde{L}_j \tag{36}$$

where $\widetilde{L}_j$ is an integer number for each $j = 1, \ldots, \widetilde{N}_c$. Define

$$\widetilde{V}_0 = \text{span}\{\widetilde{\Phi}_{j,m} : 1 \leq j \leq \widetilde{N}_c \text{ and } 1 \leq m \leq \widetilde{L}_i\}. \tag{37}$$

Define also the coarse interpolation $\widetilde{I}_0 : V^h(D) \to \widetilde{V}_0$ by

$$\widetilde{I}_0 v = \sum_{j=1}^{\widetilde{N}_c}\sum_{m=1}^{\widetilde{L}_j}\left(\int_{\widetilde{\omega}_j}\kappa(J_0^{\widetilde{\omega}_j}v)\widetilde{\psi}_m^{\widetilde{\omega}_j}\right) I^h(\widetilde{\chi}_j\widetilde{\psi}_m^{\widetilde{\omega}_j}) = \sum_{j=1}^{\widetilde{N}_c} I^h\left(\widetilde{\chi}_j I_{\widetilde{L}_j}^{\widetilde{\omega}_j}(J_0^{\widetilde{\omega}_j}v)\right), \tag{38}$$

where

$$I_{\widetilde{L}_j}^{\widetilde{\omega}_j}(J_0^{\widetilde{\omega}_j}v) = \sum_{m=1}^{\widetilde{L}_j}\left(\int_{\widetilde{\omega}_j}\kappa(J_0^{\widetilde{\omega}_j}v)\widetilde{\psi}_m^{\widetilde{\omega}_j}\right)\widetilde{\psi}_m^{\widetilde{\omega}_j}$$

and $J_0^{\widetilde{\omega}_j}v \in V_0^{\widetilde{\omega}_j}$ is defined by

$$J_0^{\widetilde{\omega}_j}v = \sum_{y_i\in\widetilde{\omega}_j}\sum_{\ell=1}^{L_i}\left(\int_{\omega_i\cap\widetilde{\omega}_j}\kappa v\psi_\ell^{\omega_i\cap\widetilde{\omega}_j}\right) I^h(\chi_i\psi_\ell^{\omega_i\cap\widetilde{\omega}_j}) \tag{39}$$

and it is the analogous to I_0 defined in (38) but restricted to the coarse block neighborhood $\widetilde{\omega}_j$.

We have the following weighted L^2 approximation and weighted H^1 stability properties.

Lemma 4 *For all coarse element $\widetilde{K} \in \mathcal{T}^{\widetilde{H}}$ we have*

$$\int_{\widetilde{K}} \kappa(v - \widetilde{I}_0 v)^2 \preceq \frac{1}{\widetilde{\lambda}_{\widetilde{K},\widetilde{L}_j+1}} \max\{1, \frac{1}{H^2 \lambda_{\widetilde{\omega}_{\widetilde{K}},L+1}}\} \int_{\widetilde{\omega}_{\widetilde{K}}} \kappa |\nabla v|^2 \tag{40}$$

$$\int_{\widetilde{K}} \kappa |\nabla \widetilde{I}_0 v|^2 \preceq \max\{1, \frac{1}{\widetilde{H}^2 \widetilde{\lambda}_{\widetilde{K},\widetilde{L}_j+1}}\} \max\{1, \frac{1}{H^2 \lambda_{\widetilde{\omega}_{\widetilde{K}},L+1}}\} \int_{\omega_{\widetilde{K}}} \kappa |\nabla v|^2 \tag{41}$$

where $\lambda_{\widetilde{\omega}_{\widetilde{K}},L+1} = \min_{y_i \in \widetilde{\omega}_{\widetilde{K}}} \lambda^{\omega_i}_{L_i+1}$ and $\widetilde{\lambda}_{\widetilde{K},\widetilde{L}+1} = \min_{\widetilde{z}_j \in \widetilde{K}} \lambda^{\widetilde{\omega}_m}_{\widetilde{L}_m+1}$ and $\widetilde{\omega}_{\widetilde{K}}$ is the union of the elements in $\mathcal{T}^{\widetilde{H}}$ that share common edge with $\widetilde{K}$ defined in (33).

The proof of this lemma is not difficult and follow from the argument in [18].

A.1.2 Discussion

We note that the computation of the eigenvector on a coarse grid does not decrease the dimension of the coarse space. i.e., the number of the eigenvectors corresponding to small, asymptotically vanishing eigenvalues, is the same whether the eigenvalue problem is solved on a fine or a coarse grid. To demonstrate this, we present two numerical examples. In the first example, we consider the computation of the eigenvector in 3×3 coarse block such that each coarse block contains an inclusion (see Figure 10). As we observe from Figure 11, there are 9 small, asymptotically vanishing, eigenvalues. Note that this is also true if the eigenvalue problem is solved on a fine (resolved) grid. In Figure 11, we also depict the eigenvalues corresponding to the fine-scale problem. As we observe there are also 9 small, asymptotically vanishing, eigenvalues. In Figure 12, we depict the eigenvector corresponding to one of the small eigenvalues computed on a coarse and fine grid. We observe that these eigenvalues are close. In fact, the error in the computation of small eigenvalues in weighted energy norm is less than 1%. In Figure 13, we depict the eigenvalues for permeability shown in Figure 3. The eigenvalue problem is solved on 10×10 coarse grid, while the fine grid is 100×100. As we observe from this figure that there are 37 small, asymptotically vanishing, eigenvalues. This is the same if the eigenvalue problem is solved on a fine grid, 100×100.

References

[1] J. E. Aarnes, *On the use of a mixed multiscale finite element method for greater flexibility and increased speed or improved accuracy in reservoir simulation*, SIAM MMS, 2 (2004), pp. 421–439.

[2] J. E. Aarnes, Y. Efendiev, and L. Jiang, *Analysis of Multiscale Finite Element Methods using Global Information For Two-Phase Flow Simulations*, SIAM MMS, 2008.

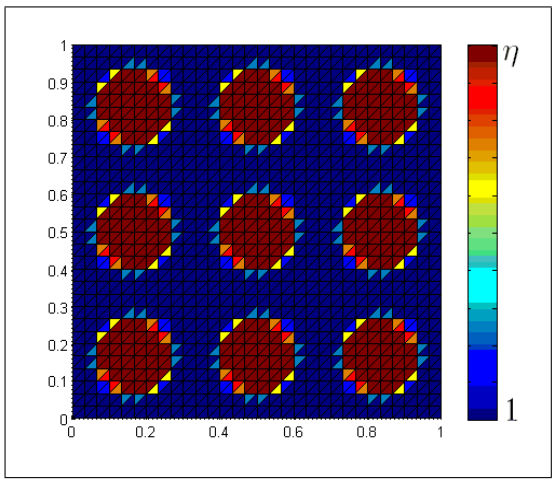

Figure 10: Permeability field.

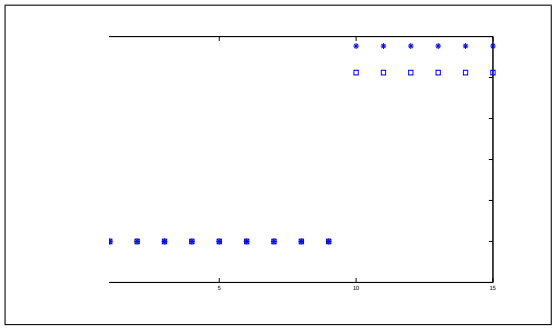

Figure 11: Eigenvalues for the conductivity field depicted in Figure 10 computed on a coarse grid (green) and a fine grid (red).

[3] J. Aarnes and T. Hou, *Multiscale domain decomposition methods for elliptic problems with high aspect ratios*, Acta Math. Appl. Sin. Engl. Ser., 18(1):63–76, 2002.

[4] J. E. Aarnes, S. Krogstad, and K.-A. Lie, *A hierarchical multiscale method for two-phase flow based upon mixed finite elements and nonuniform grids*, Multiscale Model. Simul. 5(2) (2006), pp. 337–363.

[5] T. Arbogast, *Implementation of a locally conservative numerical subgrid upscaling scheme for two-phase Darcy flow*, Comput. Geosci., 6 (2002), pp. 453–481.

[6] T. Arbogast, G. Pencheva, M. F. Wheeler, and I. Yotov, *A multiscale mortar mixed finite element method*, SIAM J. Multiscale Modeling and Simulation, 6(1), 2007, pp. 319-346

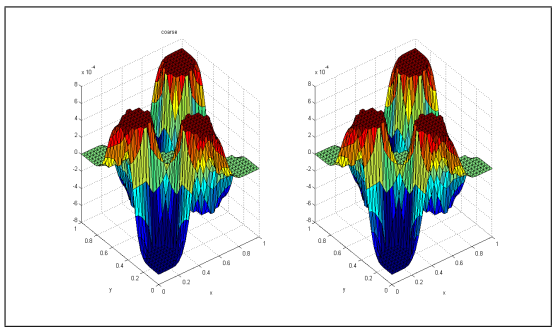

Figure 12: An eigenvector corresponding to small eigenvalue computed on a coarse grid (left) and on a find grid (right).

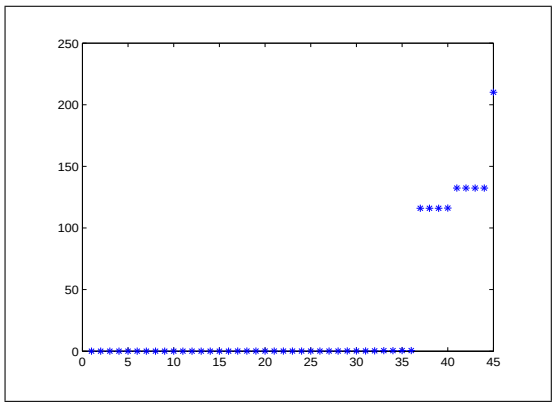

Figure 13: The eigenvalues computed by solving the problem on a coarse 10×10 coarse grid for permeability depicted in Figure 3.

[7] L. Berlyand and H. Owhadi, A new approach to homogenization with arbitrary rough high contrast coeffcients for scalar and vectorial problems. Submitted.

[8] S.C. Brenner and L.R. Scott, *The mathematical theory of finite element methods*, vol. 15 of Texts in Applied Mathematics, Springer-Verlag, New York, 1994.

[9] T. Chartier, R. Falgout, V.E. Henson, J. Jones, T. Manteuffel, S. McCormick, J. Ruge, and P.S. Vassilevski, *Spectrak AMGe*, SIAM SCI, 25 (2003), 1-26

[10] Y. Chen, L.J. Durlofsky, M. Gerritsen, and X.H. Wen, *A coupled local-global upscaling approach for simulating flow in highly heterogeneous formations*, Advances in Water Resources, 26 (2003), pp. 1041–1060.

[11] Z. Chen and T.Y. Hou, *A mixed multiscale finite element method for elliptic problems with oscillating coefficients*, Math. Comp., 72 (2002), pp.541–576 (electronic).

[12] C.C. Chu, I.G. Graham, and T.Y. Hou, *A new multiscale finite element methods for high-contrast elliptic interface problem*, submitted

[13] Y. Efendiev, V. Ginting, T. Hou, and R. Ewing, *Accurate multiscale finite element methods for two-phase flow simulations*, J. Comp. Physics, 220 (1), pp. 155-174, 2006.

[14] Y. Efendiev and T. Hou, *Multiscale finite element methods. Theory and applications*. Springer, 2009.

[15] Y. Efendiev, T. Hou, and V. Ginting, *Multiscale finite element methods for nonlinear problems and their applications*, Comm. Math. Sci., 2 (2004), pp. 553–589.

[16] Y. Efendiev, T. Y. Hou, and X. H. Wu, *Convergence of a nonconforming multiscale finite element method*, SIAM J. Num. Anal., 37 (2000), pp. 888–910.

[17] J. Galvis and Y. Efendiev, Domain decomposition preconditioners for multiscale flows in high contrast media, submitted.

[18] Y. Efendiev and J. Galvis, Domain decomposition preconditioners for multiscale flows, submitted.

[19] I. G. Graham, P. O. Lechner, and R. Scheichl, *Domain decomposition for multiscale PDEs*. Numer. Math., 106(4):589–626, 2007.

[20] I. G. Graham and R. Scheichl, *Robust domain decomposition algorithms for multiscale PDEs*, Numer. Methods Partial Differential Equations, 23(4):859–878, 2007.

[21] I. Lunati and P. Jenny, *Multi-scale finite-volume method for highly heterogeneous porous media with shale layers*, in: Proceedings of the 9th European Conference on the Mathematics of Oil Recovery (ECMOR), Cannes, France, 2004.

[22] T. P. A. Mathew, *Domain decomposition methods for the numerical solution of partial differential equations*, volume 61 of *Lecture Notes in Computational Science and Engineering*. Springer-Verlag, Berlin, 2008.

[23] T.Y. Hou and X.H. Wu, *A multiscale finite element method for elliptic problems in composite materials and porous media*, Journal of Computational Physics, 134 (1997), pp. 169–189.

[24] T. Hughes, G. Feijoo, L. Mazzei, and J. Quincy, *The variational multiscale method - a paradigm for computational mechanics*, Comput. Methods Appl. Mech. Engrg, 166 (1998), pp. 3–24.

[25] P. Jenny, S.H. Lee, and H. Tchelepi, *Multi-scale finite volume method for elliptic problems in subsurface flow simulation*, J. Comput. Phys., 187 (2003), pp. 47–67.

[26] H. Owhadi and L. Zhang, *Metric based up-scaling*, Comm. Pure Appl. Math., Comm. Pure and Applied Math., vol. LX:675-723, 2007.

[27] A. Toselli and O. Widlund. *Domain decomposition methods—algorithms and theory*, volume 34 of *Springer Series in Computational Mathematics*. Springer-Verlag, Berlin, 2005.

[28] P.S. Vassilevski, *Multilevel block factorization preconditioners. Matrix-based analysis and algorithms for solving finite element equations*, Springer, 2008

[29] J. Xu and L. Zikanov. On an energy minimizing basis for algebraic multigrid methods. *Comput Visual Sci*, 7:121–127, 2004.

[30] J. Xu and J. Zou. Some nonoverlapping domain decomposition methods. *SIAM Rev.*, 40(4):857–914 (electronic), 1998.